energies

MDPI

Article

Ruthenium (Ru) doped Titanium Dioxide (P25) Electrode for Dye Sensitized Solar Cells

Tharmakularasa Rajaramanan [1,2,3], Muthukumarasamy Natarajan [4], Punniamoorthy Ravirajan [2], Meena Senthilnanthanan [3,*] and Dhayalan Velauthapillai [1,*]

[1] Faculty of Engineering and Science, Western Norway University of Applied Sciences, P.O. Box 7030, 5020 Bergen, Norway; rramanan9@gmail.com
[2] Clean Energy Research Laboratory, Department of Physics, University of Jaffna, Jaffna 40000, Sri Lanka; pravirajan@univ.jfn.ac.lk
[3] Department of Chemistry, University of Jaffna, Jaffna 40000, Sri Lanka
[4] Department of Physics, Coimbatore Institute of Technology, Coimbatore, Tamil Nadu 641014, India; vishnukutty2002@yahoo.co.in
* Correspondence: meena@univ.jfn.ac.lk (M.S.); Dhayalan.Velauthapillai@hvl.no (D.V.); Tel.: +94-777-146-469 (M.S.); +47-5558-7711 (D.V.)

Received: 28 February 2020; Accepted: 22 March 2020; Published: 25 March 2020

Abstract: In this study, P25-titanium dioxide (TiO_2) was doped with ruthenium (Ru) by systematically varying the Ru content at 0.15, 0.30, 0.45 and 0.6 mol%. The synthesized Ru-doped TiO_2 nanomaterials have been characterized by X-ray diffraction (XRD), Raman spectroscopy, energy-dispersive X-ray (EDX) analysis, UV-visible (UV–Vis) spectroscopy, and electrochemical impedance (EIS) spectroscopy. The XRD patterns of undoped and Ru-doped TiO_2 nanomaterials confirm the presence of mixed anatase and rutile phases of TiO_2 while EDX spectrum confirms the presence of Ti, O and Ru. Further, UV-visible absorption spectra of doped TiO_2 nanomaterial reveal a slight red shift on Ru-doping. The short circuit current density (J_{SC}) of the cells fabricated using the Ru-doped TiO_2 photoanode was found to be dependent on the amount of Ru present in TiO_2. Optimized cells with 0.3 mol% Ru-doped TiO_2 electrodes showed efficiency which is 20% more than the efficiency of the control cell (η = 5.8%) under stimulated illumination (100 $mWcm^{-2}$, 1 sun) with AM 1.5 filter. The increase in J_{SC} resulted from the reduced rate of recombination upon doping of Ru and this was confirmed by EIS analysis.

Keywords: dye sensitized solar cells; Ru-doped TiO_2; P25-TiO_2

1. Introduction

Dye-sensitized solar cells (DSSCs) have been studied intensively as an alternative energy source due to their low cost, easy fabrication and more environmentally friendly nature. A DSSC consists of an electron transporting mesoporous metal oxide layer on a transparent conducting oxide coated glass, dye, electrolyte and a counter electrode. Generally, the visible light is converted into electricity in DSSCs through spectral sensitization of wide bandgap semiconductors such as SnO_2 [1], $SrTiO_3$ [2], Nb_2O_5 [3], ZnO [4] and TiO_2 [5]. Among the semiconductors explored for DSSCs so far, TiO_2 remains the most promising material [1]. Although natural dyes used as sensitizers in DSSC are cheap compared to synthetic dyes, their reported efficiencies are rather low [6-9]. The concept of a dye-sensitized solid-state solar cell was first proposed by Tennakone et al. in 1988 [10] and then O'Regan and Grätzel reported an efficiency of 7.1% and a current density greater than 12 $mAcm^{-2}$ for DSSC in which I^-/I_3^- redox couple and TiO_2 were used as liquid electrolyte and ETM, respectively [5]; later, the maximum efficiency of 11.1% was reported by Nazeeruddin et al. [11,12]. However, relaxation of oxidized dye and recombination processes connected to the charge carriers hinder the

performance of DSSCs. One of the alternative strategies to reduce the above said problem in DSSCs is the use of doped TiO_2 electrode. It is evident that dopant materials narrow the bandgap and increase the charge traps of TiO_2 and hence modify the properties, such as conduction band energy, charge transport, recombination and collection of charge carriers [13]. Different dopants, such as transition metals, alkali earth metals [14,15], non-metals [16,17], and rare earth elements [14,18], have been employed; but the incorporation of transition metals into TiO_2 gives rise to the formation of a wide range of new energy levels arising from the partially filled d-orbitals of transition metals close to the conduction band (CB) of TiO_2, that leads to a reduction in the bandgap and enhancement in harvesting visible light. This makes transition metals suitable for tuning the CB structure [13].

Various transition metals (Ag [19,20], Co [21], Mn [21], Zn [22], Cr [23], Nb [24], W [25], Cu [26], Y [27] and Sc [28]) have been used as dopant in TiO_2. Ruthenium (Ru) appears to be a good dopant as the Ru^{4+} ion has an ionic radius of 0.062 nm which is comparable to that of Ti^{4+} ion (0.061 nm) [29]. The utilization of Ru-doped TiO_2 as ETM in DSSCs has not yet been studied in depth. In 2009, Houskova et al. reported that Ru-doping decreases the bandgap of TiO_2 [30], while a contradictory observation was reported by Kong et al. in 2015 [31]. In another study, So and co-workers (2012) reported η of 5.2% using 0.02 at.% Ru-doped TiO_2 nanotube layers in DSSC [32]. Lu et al. (2016) achieved η of 5.39% for the Ru-doped TiO_2 [33]. However, the use of Ru-doped P25-TiO_2 (Degussa P25—commercially purchased TiO_2 nanopowder) as a mesoporous metal oxide in DSSCs has not been reported so far, although Ru-doped P25-TiO_2 has been widely employed to enhance photocatalytic activities [34-36].

In this study, $RuCl_3.xH_2O$ was used as a precursor to synthesize Ru-doped electrodes and their performances in DSSCs were investigated by systematically varying the Ru content. The synthesised Ru-doped TiO_2 was characterized by XRD, Raman, UV–visible, EDX and EIS spectroscopy studies.

2. Materials and Methods

2.1. Materials

All reagents and solvents used were obtained from commercial sources; absolute ethanol (>99%, Sigma Aldrich), Triton TM X-100 (laboratory grade, Sigma-Aldrich), ruthenium (III) chloride hydrate (Reagent Plus-grade, Sigma-Aldrich), titanium dioxide nanopowder (21 nm primary particle size, ≥99.5% trace metals basis, Sigma-Aldrich), di-tetrabutylammonium cis-bis(isothiocyanato)bis(2,2′-bipyridyl-4,4′-dicarboxylato)ruthenium(II) dye (95%, Sigma-Aldrich), acetonitrile (Gradient grade, Sigma-Aldrich), tert-butyl alcohol (≥99.7%, Sigma-Aldrich), acetylacetone (≥99.5%, Fluka Analytical).

2.2. Methods

2.2.1. Preparation of Ru-doped TiO_2 Nanomaterials

To achieve a reproducible outcome and comparison, a simple doping of Ru in P25-TiO_2 was used to prepare Ru-doped TiO_2 nanomaterials. Then 0.15, 0.3, 0.45 and 0.6 mol% of $RuCl_3.xH_2O$ were added to the TiO_2 nanopowder (P25) and stirred vigorously for one hour at room temperature (step 1, 2) and then it was dried at 100 °C with continuous stirring for 2 hours (step 3). The product was ground well (step 4) and the resulting Ru-TiO_2 powder mixtures were annealed at 500 °C for 3 h (step 5) (Figure 1) [26,35,37,38].

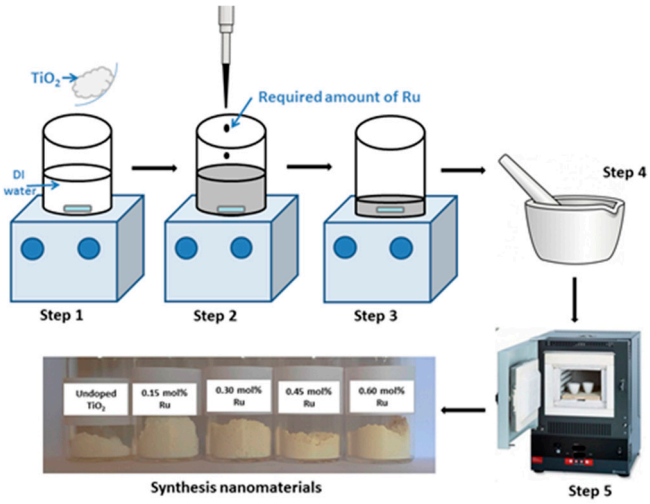

Figure 1. Schematic diagram of the synthesis of Ru-doped TiO_2 nanomaterial.

2.2.2. Fabrication of DSSCs

The fluorine-doped tin oxide (FTO) coated conducting glass (sheet resistance 7.5 Ω/cm²) was used as the current collector. It was cleaned initially with soap water and subsequently with distilled water and ethanol using an ultrasonic bath. Then, the synthesized Ru-doped TiO_2 nanomaterial was made into paste by mixing with deionized water, acetylacetone and Triton TM X-100 binder and coated on FTO by the doctor-blade technique using a glass rod with adhesive tapes (3 M Scotch tapes) as spacers and the thickness of the TiO_2 film was about 7 μm. The prepared Ru-doped TiO_2 films were dried and calcinated at 500 °C for 30 minutes. Then the coated glasses were soaked in 0.3 mM solution of N719 dye in acetonitrile/tert-butyl alcohol (50%v/v) for 12 h. After the dye-sensitization process, the photoanode was washed with acetonitrile to remove the unanchored dye molecules and dried. A platinum-coated FTO glass plate was used as the counter electrode. The dye-coated Ru-doped TiO_2 electrode and Pt counter electrode [26] were used to assemble the cell and I^-/I_3^- electrolyte was used as redox electrolyte.

2.2.3. Characterization

The structural properties of the synthesized nanomaterials were studied by the X-ray diffraction method using scan range (2θ) between 20° and 95° with step size of 0.02° and scan speed of 1°/min. A Raman spectroscopic study was carried out using a laser confocal Raman microscope (Renishaw, UK, Model: Invia). The optical absorbance spectra were recorded using Shimadzu 1800 Scanning Double Beam UV-visible spectrophotometer. The elemental composition of the synthesized nanomaterials was analyzed by the energy-dispersive X-ray spectroscopy technique. The photovoltaic performance of the cells was studied using Keithley-2400 source measurement unit (SMU) under simulated irradiation of intensity 100 $mWcm^{-2}$ with AM 1.5 filter (Peccell-PEC-L12, Japan). Current–voltage (I–V) characteristics in the dark were measured before and after the illumination which confirmed no change in device behaviour [39,40]. The effective area of the photoelectrode was 0.25 cm². Electrochemical impedance spectroscopy (EIS) measurements were carried out on the DSSCs using Metrohm Autolab potentiostat/galvanostat (PGSTAT 128N) with a frequency response analyzer (FRA 32M).

3. Results and Discussion

3.1. X-ray Siffraction and Raman Spectroscopy

The crystal structure of the synthesized nanomaterials was investigated by the X-ray diffraction method (XRD). Figure 2 represents the XRD patterns of undoped TiO_2 electrode, 0.15, 0.3, 0.45 and 0.6 mol% Ru-doped TiO_2 electrodes and diffraction peaks for 2θ diffraction angles were monitored

between 20° and 80°. The major peaks are observed at 25.2°, 37.6°, 48.2°, 53.7°, 55°, 62.5°, 68.5°, 70.2° and 74.89° and they correspond to the reflection planes of (101), (004), (200), (105), (211), (204), (116), (220) and (215) which confirms the presence of well-crystallized pure anatase TiO_2 phase and peaks at 27.39°, 36.07° and 41.2° correspond to the reflection planes of (110), (101) and (111) for minor rutile TiO_2 phase. This indicates that the anatase and rutile crystal structures are retained even after the TiO_2 being doped with Ru. The average crystallite size was calculated by the Scherrer Equation [15]

$$d = \frac{k\lambda}{BCos\theta} \quad (1)$$

where d is the crystallite size, k is a dimensionless shape factor which has a typical value of about 0.89, λ is the X-ray wavelength of Cu (0.5406 nm), θ is the Bragg angle corresponding to the anatase (101) peak, and B is the line broadening at half the maximum intensity (FWHM). The average crystallite size of undoped TiO_2, 0.15, 0.3, 0.45 and 0.6 mol% Ru-doped TiO_2 nanomaterials were 17.34, 17.34, 17.79, 17.56 and 17.34 nm and no significant change was observed in the crystallite size. Phase transformation from anatase to rutile was not observed on Ru-doping and hence the crystallite size remains the same. Ismael et al. reported that doping of Ru into the TiO_2 lattice does not change the TiO_2 crystal structure but the predominant anatase peaks of Ru-doped TiO_2 are shifted slightly towards lower 2θ values when the ruthenium dopant is incorporated in TiO_2 lattice [41]. Ionic radii of Ru^{4+} and Ti^{4+} are 0.062 and 0.061 nm, respectively. As both the ions have almost the same ionic radii, in the Ru-doped TiO_2, the incorporated ruthenium ions may be substituting for titanium ions in the lattice. However, crystallite peaks of Ru could not be clearly observed in Ru-doped TiO_2 which may be due to low mol% of the dopant and similar observations have been reported by Senthilnanthan et al. (2010) and Elezović et al. (2013) [35,42].

Figure 3a shows the Raman spectra obtained for the undoped TiO_2 and Ru-doped TiO_2 nanomaterials. The Raman spectrum of the undoped TiO_2 nanoparticles was dominated with five bands corresponding to the six Raman active modes. Well resolved TiO_2 Raman peaks with the D_{4h} space group at about 170, 216, and 657 cm^{-1} (E_g), 539 cm^{-1} ($A_{1g} + B_{1g}$), and 420 cm^{-1} (B_{1g}) were observed which correspond to the anatase phase of TiO_2 [43]. Figure 3b shows that the peak intensity became weak and also the peak became broader with the increase in the percentage of Ru-doping. In general, the Raman line shape, intensity and position are strongly influenced by lattice strain, defects, and the crystallite size and shape. There was no peak for the Ru and the same behaviour is observed in the XRD studies. This suggests that Ru ions have been successfully incorporated in the TiO_2 lattice.

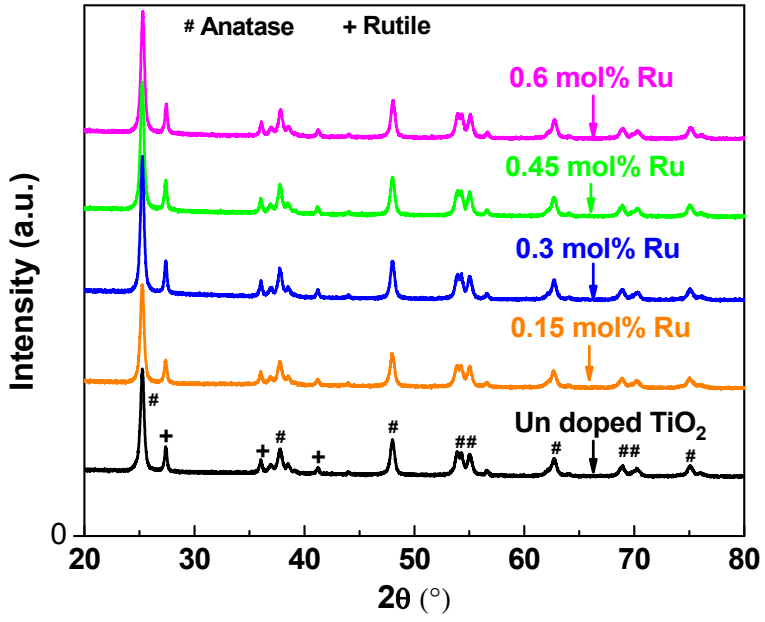

Figure 2. XRD patterns of undoped TiO_2, 0.15, 0.3, 0.45 and 0.6 mol% Ru-doped TiO_2 nanomaterials.

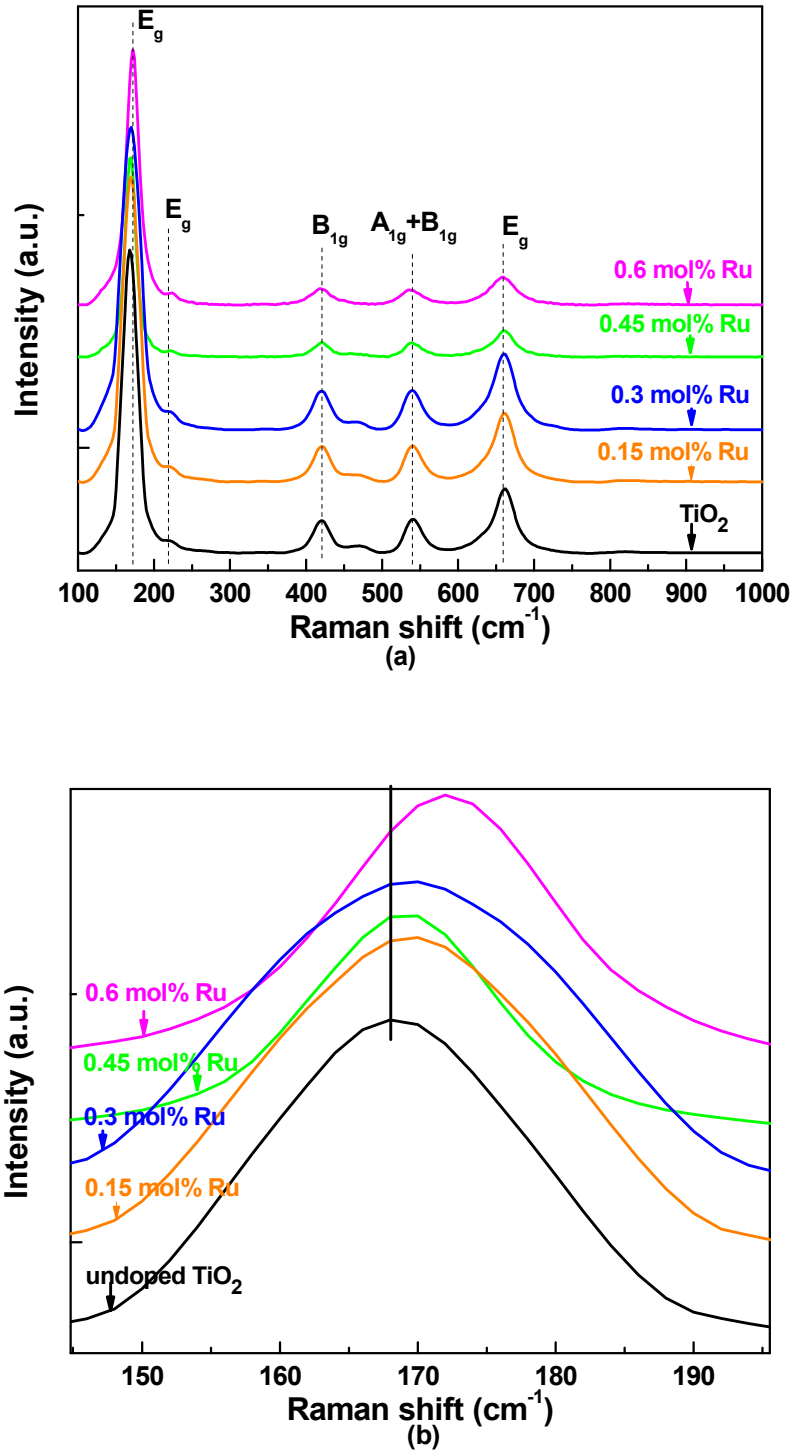

Figure 3. (**a**) Raman spectra of undoped TiO_2, 0.15, 0.3, 0.45 and 0.6 mol% Ru-doped TiO_2 nanomaterials; (**b**) Detailed E_g-170 cm^{-1} Raman peaks of undoped TiO_2 and Ru-doped TiO_2 nanomaterials.

3.2. UV–visible Absorption Spectroscopy

UV–visible spectroscopy was employed to study the optical properties of the prepared nanomaterials. Five milligrams of the nanomaterial was dispersed in 100 ml of the deionized water in an ultrasonic bath and 1 ml of the dispersed sample was transferred to a standard quartz cuvette

for measurement [23]. Figure 4a represents the optical absorption spectra of undoped TiO_2, 0.15, 0.3, 0.45 and 0.6 mol% Ru-doped TiO_2 nanomaterials. As can be seen from Figure 4a the absorption peak of undoped TiO_2 nanomaterial appears in the UV region whereas there is a slight red shift in the absorption spectrum of Ru-doped TiO_2 and this red shift is found to increase with the increase in Ru-doping indicating the bandgap narrowing due to the introduction of a mid-bandgap or impurity levels located between the valence band and the conduction band of TiO_2. In addition, the light absorption in the range from 400 to 700 nm is found to increase with increasing Ru content in the Ru-doped TiO_2, accompanied with a change in the colour from white to reddish black [41]. The bandgap (E_g) of undoped TiO_2, 0.15, 0.3, 0.45 and 0.6 mol% Ru-doped TiO_2 nanomaterials was calculated using Tauc plots, where the intercept of the tangent to the plot $(\alpha h\upsilon)^2$ versus $h\upsilon$ gives a good estimation of the direct bandgap for a semiconductor. The optical absorbance coefficient of a semiconductor for direct transition is given by the equation

$$\alpha = A\frac{\left(h\upsilon - E_g\right)^n}{h\upsilon} \quad (2)$$

where $h\upsilon$ = photon energy, α = absorbance coefficient, E_g = bandgap energy, A = constant and the exponent 'n' depends on the type of transition and it may have values of 1/2, 2, 3/2 and 3, corresponding to the allowed direct, allowed indirect, forbidden direct and forbidden indirect transitions, respectively. As shown in the Figure 4b, undoped TiO_2, 0.15, 0.3, 0.45 and 0.6 mol% Ru-doped TiO_2 nanomaterials have bandgap values of 3.16, 3.12, 3.05, 3.02 and 2.98 eV, respectively (straight-line intercept to the energy axis). The reduction in bandgap can be attributed to the insertion of Ru into the TiO_2 lattice. Since the lower edge of the CB is made up of Ti^{4+} 3d bands [15], the substitution of Ti^{4+} with the Ru cation might have affected the CB structure. A similar observation has been reported by Wang et al., Lu et al. and Ismael et al. [29,33,41].

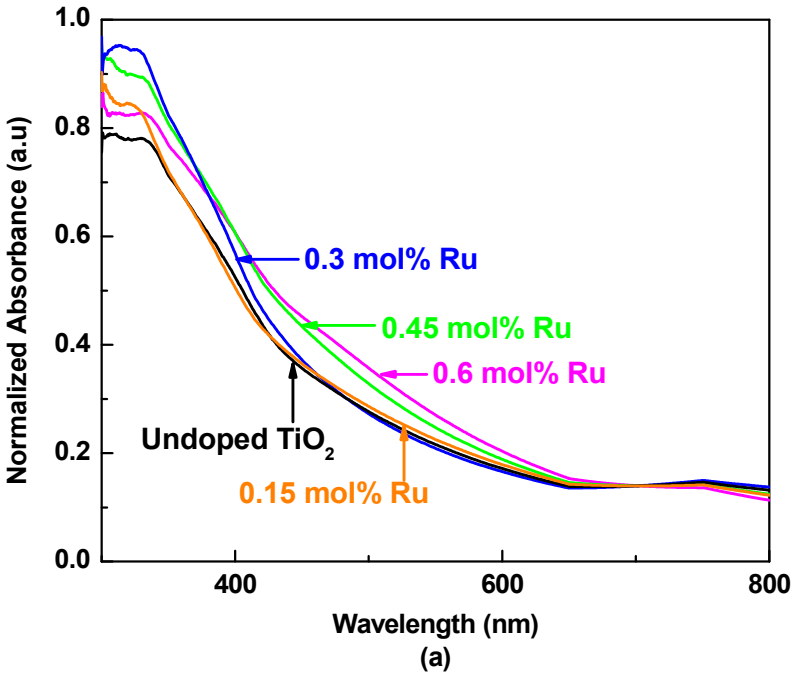

(a)

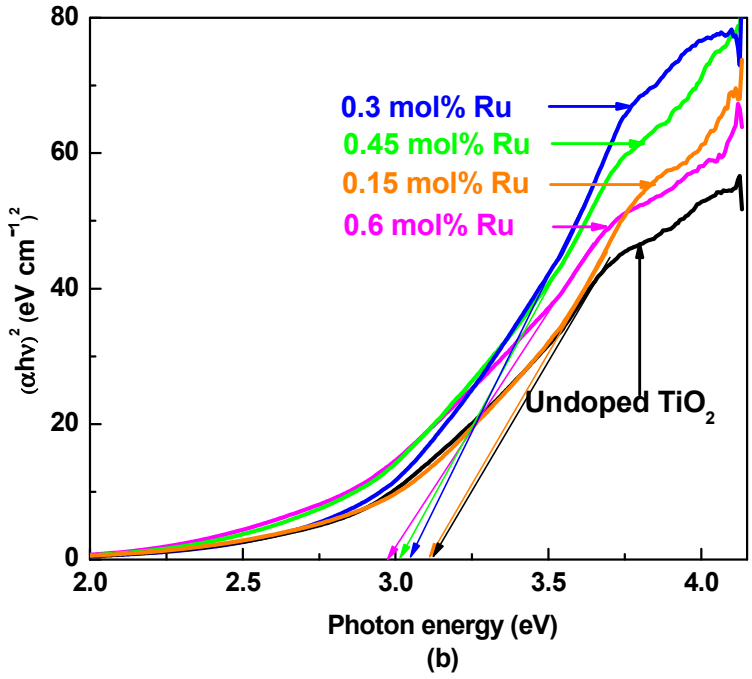

Figure 4. (**a**) UV–visible absorption spectra of undoped TiO_2, 0.15, 0.3, 0.45 and 0.6 mol% Ru-doped TiO_2 nanomaterials; (**b**) Plot of $(\alpha h\upsilon)^2$ versus Photon energy for undoped TiO_2, 0.15, 0.3, 0.45 and 0.6 mol% Ru-doped TiO_2 nanomaterials.

3.3. Energy-Dispersive X-ray Spectroscopy

Figure 5 illustrates the elemental analysis of the undoped and Ru-doped TiO_2 samples, studied using energy-dispersive X-ray spectroscopy in the binding energy region of 0.0–20.0 KeV and the results are summarized in Table 1, which reveals the existence of Ti, O and Ru elements in Ru-doped TiO_2.

Table 1. Atomic percentage of Ru-doped TiO_2 in terms of energy-dispersive X-ray (EDX) investigation.

Samples	EDX Result-Ru at. %
Undoped TiO_2 (a)	0
0.15 mol% Ru (b)	0.10
0.30 mol% Ru (c)	0.25
0.45 mol% Ru (d)	0.46
0.60 mol% Ru(e)	0.75

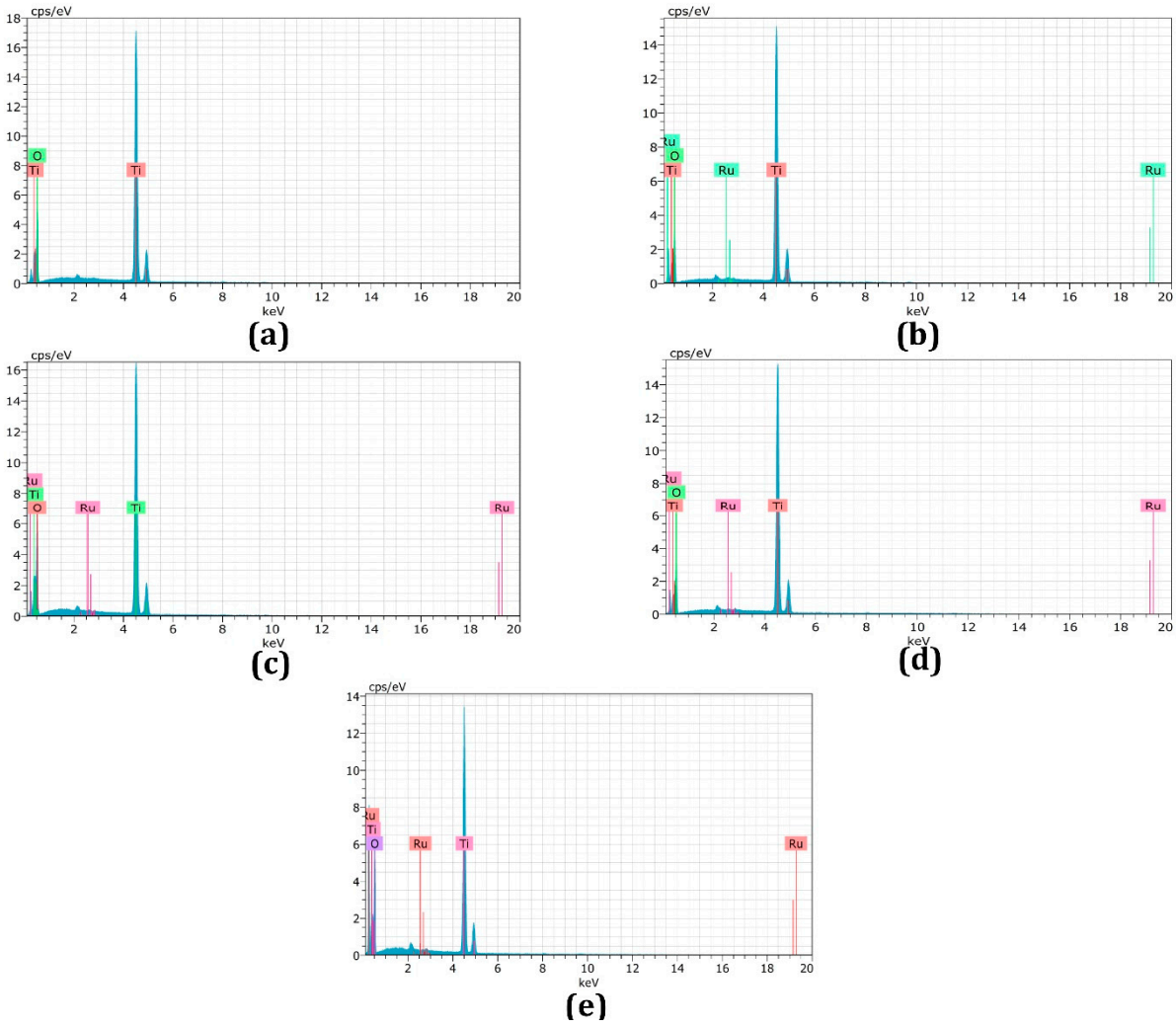

Figure 5. (**a**–**e**) EDX spectra of undoped and 0.15, 0.3, 0.45, 0.6 Ru-doped TiO_2 nanomaterials in the binding energy region from 0.0 to 20.0 KeV.

3.4. J–V Characteristics

Figure 6a represents the J–V characteristics of DSSCs (in each type four devices were made and readings of the champion cells have been reported) made of photoanodes containing TiO_2 electrodes doped with different mol% of Ru and its control under simulated irradiation intensity of 100 $mWcm^{-2}$ with AM 1.5 filter. The corresponding photovoltaic parameters such as the short circuit current density (J_{SC}), open-circuit photovoltage (V_{OC}), fill factor (FF) and power conversion efficiency (η) of these cells with Ru-doped TiO_2 electrodes and undoped TiO_2 electrode are summarized in Table 2. Moreover, Figure 6b indicates the influence of different Ru mol% dopant on J_{SC} and η. Ru-doping produces little improvement in V_{OC} and FF. The control cell showed V_{OC} of 0.66 V, which slightly increased to 0.69 V when 0.3 mol% Ru was doped. When the mol% of Ru dopant increases, Jsc shows a slight increase from 12.9 to 14.42 $mAcm^{-2}$ up to 0.15 mol% Ru and then it attains a maximum of 14.73 mA/cm^2 for 0.3 mol% Ru, subsequently, the J_{SC} values show a downward trend with further increase in Ru mol%. A similar trend was reflected in the η versus Ru mol% plot. The overall efficiency of the cell is mainly influenced by J_{SC}. Similar observations have been reported by So and co-workers (2012) in DSSCs with Ru-doped TiO_2 nanotubes [32]. In our study, the cell fabricated with 0.3 mol% Ru-doped TiO_2 electrode showed the best η of 7% which is over 20% enhancement relative to undoped TiO_2 based DSSC (η = 5.78%).

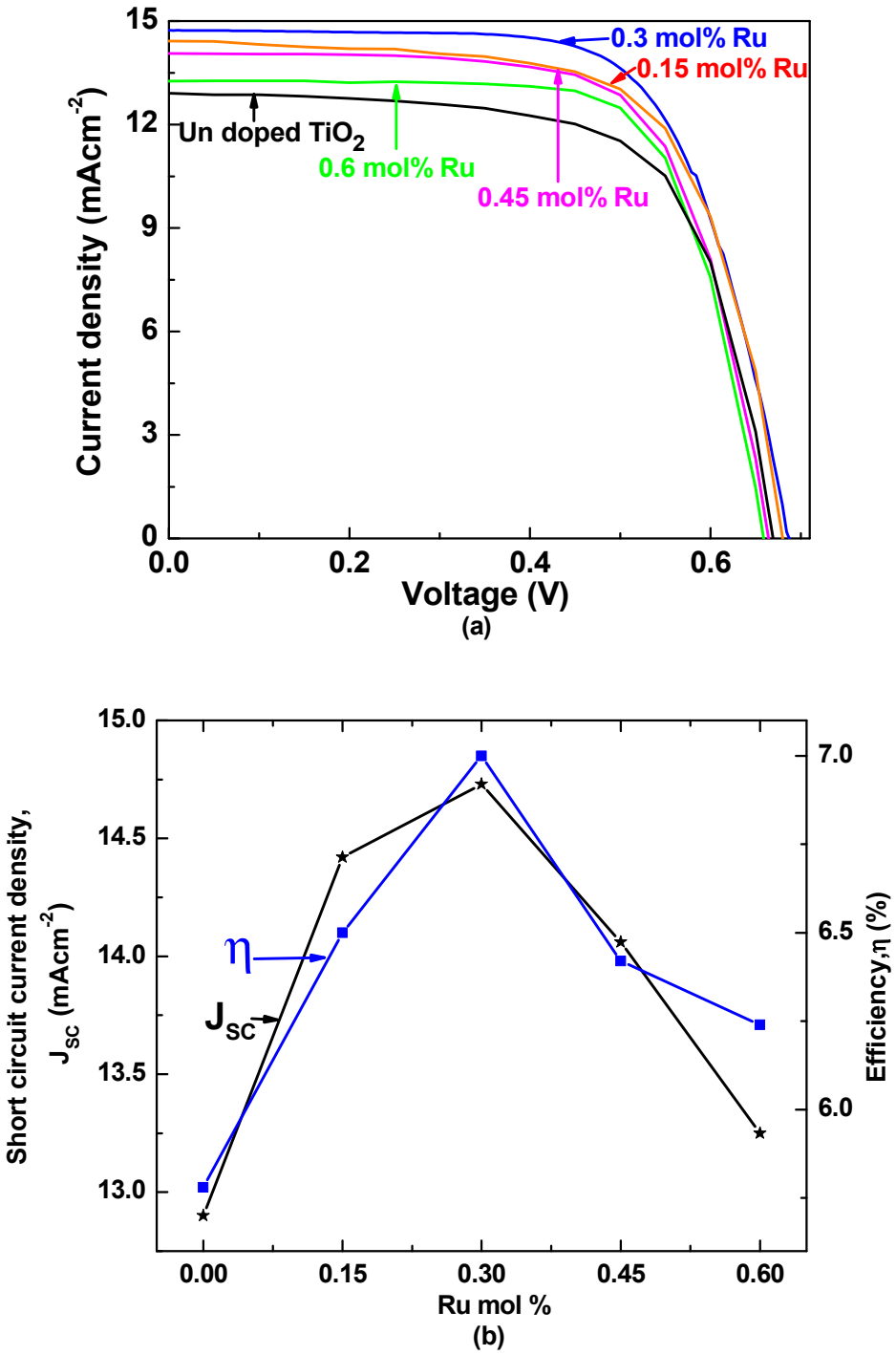

Figure 6. (**a**) Current–voltage (J–V) characteristic curves of the dye-sensitized solar cells (DSSCs) assembled with 0.15, 0.3, 0.45 and 0.6 mol% Ru-doped TiO_2 photoanodes and its control undoped TiO_2 photoanode under simulated irradiation of intensity 100 $mWcm^{-2}$ with AM 1.5 filter; (**b**) variations in Jsc and η with different mol% Ru dopants).

Table 2. Current-voltage (J–V) characteristics of the DSSCs assembled with different mol% Ru-doped P25-TiO_2 photoanodes and its control P25-TiO_2 photoanodes.

mol% of Ru in TiO_2	Jsc (mA/cm²)	Voc (V)	FF	η (%)
0.6	13.25	0.66	0.70	6.24
0.45	14.06	0.66	0.68	6.42

0.3	14.73	0.69	0.68	7.00
0.15	14.42	0.67	0.67	6.50
0	12.90	0.66	0.66	5.78

3.5. Electrochemical Impedance Spectroscopy

The interfacial charge transport phenomena of the DSSCs can be studied using electrochemical impedance spectroscopy (EIS). Figure 7 shows the Nyquist plots of the electrochemical impedance spectra of DSSCs based on the control and 0.15, 0.3, 0.45 and 0.6 mol% Ru-doped TiO_2 photoanodes, which were measured at frequencies from 10^{-2} to 10^6 Hz in the dark, with a bias applied voltage of 10 mV [24]. The small semicircle in the high-frequency range corresponds to the charge transfer resistance (R_1), which is related to the charge transfer at the interface of the electrolyte/Pt counter electrode and FTO/TiO_2 interface. A larger semicircle in the low frequency region is mainly related to the charge recombination resistance (R_2) across the TiO_2/electrolyte interface with a partial contribution from electron transport and accumulation in TiO_2 photoanode [44]. R_1 and R_2 values can be estimated from the diameter of the semicircles and resistance related to electron recombination (R_2) increases with Ru-doping up to 0.3 mol% and then it starts to decrease with the increase in concentration of Ru. The higher values of resistance related to electron recombination indicate reduced electron recombination in Ru-doped electrodes [45]. This is the reason for the higher Jsc values for the Ru-doped devices in the J–V measurement [32] even though increased recombination resistance and reduced recombination rate improve the Voc of the Ru-doped devices, this can also be attributed to the reduction in the bandgap as well [15]. A similar observation was reported by Wang et al. in perovskite solar cells [29] and also Ismael et al. (2019) reported that Ru-doping could facilitate the separation and migration of photogenerated electron–hole pairs [41].

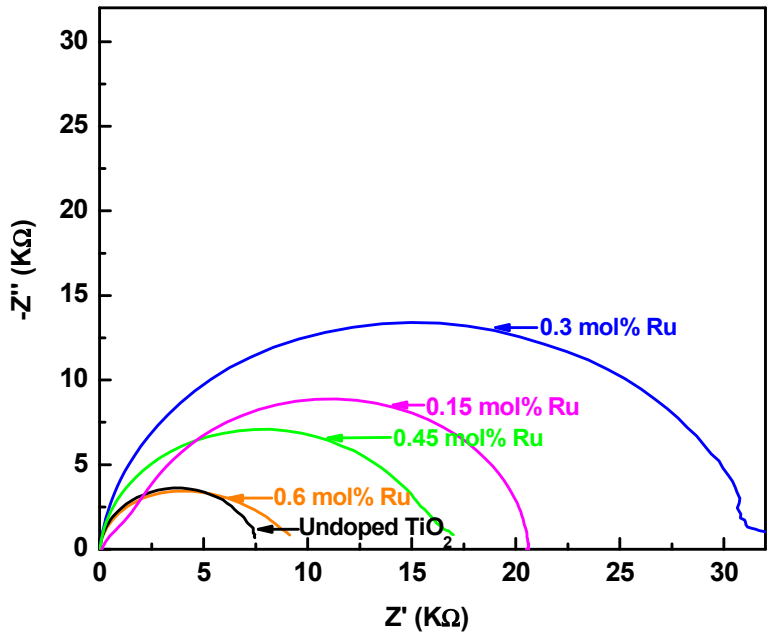

Figure 7. Nyquist plot of DSSCs with 0.15, 0.3, 0.45, 0.6 mol% Ru-doped TiO_2 photoanodes and the control cell in dark.

4. Conclusions

In the present study, Ru-doped TiO_2 electrodes were fabricated by treating TiO_2 with $RuCl_3.xH_2O$ and by systematically varying the Ru content from 0.15% to 0.6%. The XRD pattern of Ru-doped TiO_2 nanomaterial confirms the presence of mixed anatase and rutile phases of TiO_2. Optical absorption spectra of pure TiO_2 and Ru-doped TiO_2 reveal a slight red shift in the absorption spectrum upon Ru-doping. Among the DSSCs fabricated, the cell with 0.3 mol% Ru-doped TiO_2

electrode exhibited an optimum efficiency which is over 20% enhancement when compared to the control cell under stimulated AM 1.5 filter (100 $mWcm^{-2}$, 1 sun). The EIS analysis of the cells confirms that charge recombination resistance is significantly increased upon Ru-doping that effectively suppresses the charge recombination rate, which results in better electron transport in the cell.

Author Contributions: Conceptualization, M.S., P.R. and D.V.; methodology, T.R., M.S. and P.R.; formal analysis, T.R., P.R. and D.V.; resources, D.V., N.M. and P.R.; data curation, T.R., M.S., P.R. and D.V.; writing—original draft preparation, T.R.; writing—review and editing, M.S., P.R., N.M. and D.V.; supervision, M.S., P.R. and D.V.; project administration, D.V. and P.R.; funding acquisition, D.V. and P.R. All authors have read and agreed to the published version of the manuscript.

Funding: This research was funded by Capacity Building and Establishment of a Research Consortium (CBERC) project, grant number LKA-3182-HRNCET and Higher Education and Research collaboration on Nanomaterials for Clean Energy Technologies (HRNCET) project, Grant number NORPART/2016/10237.

Acknowledgments: P. Balraju, Coimbatore Institute of Technology, India for SEM measurement, Dr. K. Vignarooban, University of Jaffna, Sri Lanka for EIS measurement, Dr. Akila Yuvapragasam, PSG Institute of Technology and Applied Research, India for the critical reading of the manuscript and P.R. acknowledge National Research Council, Sri Lanka for Metrohm Autolab Potentiostat/galvanostat.

Conflicts of Interest: The authors declare no conflict of interest. The funders had no role in the design of the study; in the collection, analyses or interpretation of data; in the writing of the manuscript, or in the decision to publish the results.

References

1. Kay, A.; Grätzel, M. Dye-sensitized core− shell nanocrystals: improved efficiency of mesoporous tin oxide electrodes coated with a thin layer of an insulating oxide. *Chemistry of Materials* **2002**, *14*, 2930-2935.
2. Burnside, S.; Moser, J.-E.; Brooks, K.; Grätzel, M.; Cahen, D. Nanocrystalline mesoporous strontium titanate as photoelectrode material for photosensitized solar devices: increasing photovoltage through flatband potential engineering. *The Journal of Physical Chemistry B* **1999**, *103*, 9328-9332.
3. Sayama, K.; Sugihara, H.; Arakawa, H. Photoelectrochemical properties of a porous Nb_2O_5 electrode sensitized by a ruthenium dye. *Chemistry of Materials* **1998**, *10*, 3825-3832.
4. Saito, M.; Fujihara, S. Large photocurrent generation in dye-sensitized ZnO solar cells. *Energy & Environmental Science* **2008**, *1*, 280-283.
5. O'Regan, B.; Grätzel, M. A low-cost, high-efficiency solar cell based on dye-sensitized colloidal TiO_2 films. *nature* **1991**, *353*, 737-740.
6. Gokilamani, N.; Muthukumarasamy, N.; Thambidurai, M.; Ranjitha, A.; Velauthapillai, D. Utilization of natural anthocyanin pigments as photosensitizers for dye-sensitized solar cells. *Journal of sol-gel science and technology* **2013**, *66*, 212-219.
7. Prabavathy, N.; Balasundaraprabhu, R.; Balaji, G.; Malikaramage, A.; Prasanna, S.; Sivakumaran, K.; Kumara, G.; Rajapakse, R.; Velauthapillai, D. Investigations on the photo catalytic activity of calcium doped TiO_2 photo electrode for enhanced efficiency of anthocyanins based dye sensitized solar cells. *Journal of Photochemistry and Photobiology A: Chemistry* **2019**, *377*, 43-57.
8. Prabavathy, N.; Shalini, S.; Balasundaraprabhu, R.; Velauthapillai, D.; Prasanna, S.; Muthukumarasamy, N. Enhancement in the photostability of natural dyes for dye-sensitized solar cell (DSSC) applications: a review. *International Journal of Energy Research* **2017**, *41*, 1372-1396.
9. Senthil, T.; Muthukumarasamy, N.; Velauthapillai, D.; Agilan, S.; Thambidurai, M.; Balasundaraprabhu, R. Natural dye (cyanidin 3-O-glucoside) sensitized nanocrystalline TiO_2 solar cell fabricated using liquid electrolyte/quasi-solid-state polymer electrolyte. *Renewable Energy* **2011**, *36*, 2484-2488.
10. Tennakone, K.; Hewaparakkrama, K.; Dewasurendra, M.; Jayatissa, A.; Weerasena, L. Dye-sensitised solid-state photovoltaic cells. *Semiconductor Science and Technology* **1988**, *3*, 382.
11. Memarian, N.; Concina, I.; Braga, A.; Rozati, S.M.; Vomiero, A.; Sberveglieri, G. Hierarchically assembled ZnO nanocrystallites for high-efficiency dye-sensitized solar cells. *Angewandte Chemie International Edition* **2011**, *50*, 12321-12325.
12. Nazeeruddin, M.K.; Baranoff, E.; Grätzel, M. Dye-sensitized solar cells: a brief overview. *Solar energy* **2011**, *85*, 1172-1178.

13. Roose, B.; Pathak, S.; Steiner, U. Doping of TiO_2 for sensitized solar cells. *Chemical Society Reviews* **2015**, *44*, 8326-8349.
14. Tanyi, A.R.; Rafieh, A.I.; Ekaneyaka, P.; Tan, A.L.; Young, D.J.; Zheng, Z.; Chellappan, V.; Subramanian, G.S.; Chandrakanthi, R. Enhanced efficiency of dye-sensitized solar cells based on Mg and La co-doped TiO_2 photoanodes. *Electrochimica Acta* **2015**, *178*, 240-248.
15. Mehnane, H.F.; Wang, C.; Kondamareddy, K.K.; Yu, W.; Sun, W.; Liu, H.; Bai, S.; Liu, W.; Guo, S.; Zhao, X.-Z. Hydrothermal synthesis of TiO_2 nanoparticles doped with trace amounts of strontium, and their application as working electrodes for dye sensitized solar cells: tunable electrical properties & enhanced photo-conversion performance. *RSC Advances* **2017**, *7*, 2358-2364.
16. Yang, S.; Guo, S.; Xu, D.; Xue, H.; Kou, H.; Wang, J.; Zhu, G. Improved efficiency of dye-sensitized solar cells applied with F-doped TiO_2 electrodes. *Journal of Fluorine Chemistry* **2013**, *150*, 78-84.
17. Sun, Q.; Zhang, J.; Wang, P.; Zheng, J.; Zhang, X.; Cui, Y.; Feng, J.; Zhu, Y. Sulfur-doped TiO_2 nanocrystalline photoanodes for dye-sensitized solar cells. *Journal of Renewable and Sustainable Energy* **2012**, *4*, 023104.
18. Xing, G.; Zhang, Z.; Qi, S.; Zhou, G.; Zhang, K.; Cui, Z.; Feng, Y.; Shan, Z.; Meng, S. Effect of cerium ion modifications on the photoelectrochemical properties of TiO_2-based dye-sensitized solar cells. *Optical Materials* **2018**, *75*, 102-108.
19. Sakthivel, T.; Kumar, K.A.; Ramanathan, R.; Senthilselvan, J.; Jagannathan, K. Silver doped TiO_2 nano crystallites for dye-sensitized solar cell (DSSC) applications. *Materials Research Express* **2017**, *4*, 126310.
20. Ranjitha, A.; Muthukumarasamy, N.; Thambidurai, M.; Velauthapillai, D. Enhanced photovoltaic performance of quantum dot sensitized solar cells with Ag-doped TiO_2 nanocrystalline thin films. *Journal of Materials Science: Materials in Electronics* **2014**, *25*, 2724-2729.
21. Yacoubi, B.; Samet, L.; Bennaceur, J.; Lamouchi, A.; Chtourou, R. Properties of transition metal doped-titania electrodes: Impact on efficiency of amorphous and nanocrystalline dye-sensitized solar cells. *Materials Science in Semiconductor Processing* **2015**, *30*, 361-367.
22. Jin, E.M.; Jeong, S.M.; Kang, H.-C.; Gu, H.-B. Photovoltaic effect of metal-doped TiO_2 nanoparticles for dye-sensitized solar cells. *ECS Journal of Solid State Science and Technology* **2016**, *5*, Q109-Q114.
23. Asemi, M.; Maleki, S.; Ghanaatshoar, M. Cr-doped TiO_2-based dye-sensitized solar cells with Cr-doped TiO_2 blocking layer. *Journal of Sol-Gel Science and Technology* **2017**, *81*, 645-651.
24. Lü, X.; Mou, X.; Wu, J.; Zhang, D.; Zhang, L.; Huang, F.; Xu, F.; Huang, S. Improved-performance dye-sensitized solar cells using Nb-doped TiO2 electrodes: efficient electron injection and transfer. *Advanced Functional Materials* **2010**, *20*, 509-515.
25. Tong, Z.; Peng, T.; Sun, W.; Liu, W.; Guo, S.; Zhao, X.-Z. Introducing an intermediate band into dye-sensitized solar cells by W6+ doping into TiO_2 nanocrystalline photoanodes. *The Journal of Physical Chemistry C* **2014**, *118*, 16892-16895.
26. Wijayarathna, T.; Aponsu, G.; Ariyasinghe, Y.; Premalal, E.; Kumara, G.; Tennakone, K. A high efficiency indoline-sensitized solar cell based on a nanocrystalline TiO2 surface doped with copper. *Nanotechnology* **2008**, *19*, 485703.
27. Qu, X.; Hou, Y.; Liu, M.; Shi, L.; Zhang, M.; Song, H.; Du, F. Yttrium doped TiO_2 porous film photoanode for dye-sensitized solar cells with enhanced photovoltaic performance. *Results in Physics* **2016**, *6*, 1051-1058.
28. Latini, A.; Cavallo, C.; Aldibaja, F.K.; Gozzi, D.; Carta, D.; Corrias, A.; Lazzarini, L.; Salviati, G. Efficiency improvement of DSSC photoanode by scandium doping of mesoporous titania beads. *The Journal of Physical Chemistry C* **2013**, *117*, 25276-25289.
29. Wang, S.; Liu, B.; Zhu, Y.; Ma, Z.; Miao, X.; Ma, R.; Wang, C.-y. Enhanced performance of TiO_2-based perovskite solar cells with Ru-doped TiO_2 electron transport layer; 2018; Vol. 169, pp. 335-342.
30. Houšková, V.; Štengl, V.; Bakardjieva, S.; Murafa, N.; Tyrpekl, V. Efficient gas phase photodecomposition of acetone by Ru-doped Titania. *Applied Catalysis B: Environmental* **2009**, *89*, 613-619.
31. Kong, D.; Jin, X.; Sun, W.; Du, J.; Tong, J.; Chen, C.; Yang, X.; Cheng, Y.; Li, Q. Ruthenium cation substitutional doping for efficient charge carrier transfer in organic/inorganic hybrid solar cells. *Journal of Power Sources* **2015**, *274*, 701-708.
32. So, S.; Lee, K.; Schmuki, P. Ru-doped TiO_2 nanotubes: Improved performance in dye-sensitized solar cells. *physica status solidi (RRL) – Rapid Research Letters* **2012**, *6*, 169-171, doi:doi:10.1002/pssr.201105600.

33. Lu, W.-H.; Chou, C.-S.; Chen, C.-y.; Wu, P. Micro-and electronic structure optimization of Ru-doped TiO_2 electrodes for efficient dye-sensitized solar cells. *Solar Energy* **2016**, *139*, 318-327.
34. Ohno, T.; Tanigawa, F.; Fujihara, K.; Izumi, S.; Matsumura, M. Photocatalytic oxidation of water by visible light using ruthenium-doped titanium dioxide powder. *Journal of Photochemistry and Photobiology A: Chemistry* **1999**, *127*, 107-110.
35. Senthilnanthan, M.; Ho, D.; Vigneswaran, S.; Ngo, H.; Shon, H. Visible light responsive ruthenium-doped titanium dioxide for the removal of metsulfuron-methyl herbcide in aqueous phase. *Separation and Purification Technology* **2010**, *75*, 415-419.
36. Upadhyay, P.; Srivastava, V. Synthesis of ruthenium metal doped titanium dioxide nanoparticles for CO_2 hydrogenation. In Proceedings of AIP Conference Proceedings; p. 020074.
37. Lim, S.P.; Pandikumar, A.; Lim, H.N.; Ramaraj, R.; Huang, N.M. Boosting photovoltaic performance of dye-sensitized solar cells using silver nanoparticle-decorated N, S-Co-doped-TiO_2 photoanode. *Scientific reports* **2015**, *5*, 11922.
38. Thambidurai, M.; Foo, S.; Salim, K.M.; Harikesh, P.; Bruno, A.; Jamaludin, N.F.; Lie, S.; Mathews, N.; Dang, C. Improved photovoltaic performance of triple-cation mixed-halide perovskite solar cells with binary trivalent metals incorporated into the titanium dioxide electron transport layer. *Journal of Materials Chemistry C* **2019**, *7*, 5028-5036.
39. Loheeswaran, S.; Thanihaichelvan, M.; Ravirajan, P.; Nelson, J. Controlling recombination kinetics of hybrid poly-3-hexylthiophene (P3HT)/titanium dioxide solar cells by self-assembled monolayers. *Journal of Materials Science: Materials in Electronics* **2017**, *28*, 4732-4737.
40. Thanihaichelvan, M.; Sockiah, K.; Balashangar, K.; Ravirajan, P. Cadmium sulfide interface layer for improving the performance of titanium dioxide/poly (3-hexylthiophene) solar cells by extending the spectral response. *Journal of Materials Science: Materials in Electronics* **2015**, *26*, 3558-3563.
41. Ismael, M. High effective ruthenium-doped TiO_2 nanoparticles photocatalyst for visible-light-driven photocatalytic hydrogen production. *New Journal of Chemistry* **2019**.
42. Elezović, N.; Babić, B.; Radmilovic, V.; Vračar, L.M.; Krstajić, N. Novel Pt catalyst on ruthenium doped TiO_2 support for oxygen reduction reaction. *Applied Catalysis B: Environmental* **2013**, *140*, 206-212.
43. Madurai, V.; Natarajan, M.; Santhanam, A.; Asokan, V.; Velauthapillai, D. Size controlled synthesis of TiO_2 nanoparticles by modi fi ed solvothermal method towards e ff ective photo catalytic and photovoltaic applications. *Mater. Res. Bull.* **2018**, *97*, 351-360.
44. Thambidurai, M.; Shini, F.; Harikesh, P.; Mathews, N.; Dang, C. Highly stable and efficient planar perovskite solar cells using ternary metal oxide electron transport layers. *Journal of Power Sources* **2020**, *448*, 227362.
45. Shini, F.; Thambidurai, M.; Harikesh, P.; Mathews, N.; Huang, Y.; Dang, C. Heterogeneous electron transporting layer for reproducible, efficient and stable planar perovskite solar cells. *Journal of Power Sources* **2019**, *437*, 226907.